Theoretical and experimental studies of the H^+-N_2 system: Differential cross sections for direct and charge-transfer scattering at kilo-electron-volt energies

R. Cabrera-Trujillo, Y. Öhrn, E. Deumens, and J. R. Sabin
Quantum Theory Project, Departments of Physics and Chemistry, University of Florida, P. O. Box 118435, Gainesville, Florida, 32611-8435

B. G. Lindsay
Department of Physics and Astronomy, Rice University, 6100 Main Street, Houston, Texas 77005-1892
(Received 18 June 2002; published 21 October 2002)

Differential direct and charge-transfer scattering cross sections are calculated for collisions of H^+ with N_2 using the electron nuclear dynamics formalism. The calculated cross sections are compared to direct scattering measurements which are also reported here and to the experimental charge transfer data of Gao *et al.* [R. S. Gao, L. K. Johnson, C. L. Hakes, K. A. Smith, and R. F. Stebbings, Phys. Rev. A **41**, 5929 (1990)]. Cross sections are presented for projectile energies of 0.5, 1.5, and 5.0 keV and scattering angles of 0.01° to 10°. The differential cross section reveals considerable structure over this angular range which is a consequence of small angle quantum interference and the glory and rainbow effects. For the case of charge transfer, we find that at least 90% of charge transfer events result in the hydrogen atom leaving the system in the $H(1s)$ state.

DOI: 10.1103/PhysRevA.66.042712 PACS number(s): 34.50.−s, 34.70.+e

I. INTRODUCTION

The understanding of collision processes is of fundamental importance in many areas including fusion plasmas, gas discharge lasers, semiconductor plasma etching, planetary atmospheres and the interstellar medium. Differential scattering in ion-atom and ion-molecule collisions may be used to probe the basic interactions, potentials, and dynamical properties of the interacting system. Two of the most important of these ion-molecule processes are direct scattering, in which the charge state of the projectile does not change, and charge transfer (or electron capture). A full description of an ion-molecule collision system must take account of the dynamics of the electrons and nuclei and requires that both direct scattering and charge-transfer scattering be incorporated.

The H^+-N_2 collision system considered here, which has particular relevance to models of proton auroral precipitation into the Earth's upper atmosphere [1], has been subject to a limited number of prior theoretical and experimental studies. Moore [2] studied vibrational excitation of the N_2 target, Birely [3] and Lavrov *et al.* [4] studied formation of excited $N_2^+(B)$ charge transfer products, Loyd and Dawson [5] measured the cross section for formation of $H(3s)$ and $H(4s)$ excited neutral products, and Lee and Lin [6] measured the Balmer-series radiation produced by such collisions. Only two prior H^+-N_2 differential scattering experiments have been reported. This is typical for ion-molecule systems which have received much less attention than ion-atom systems [7]. Quintana *et al.* [8] carried out a charge transfer study for proton energies of 0.5 to 3.0 keV and found that the $H(1s)+N_2^+(X)$ channel dominates this process only at small angles. Gao *et al.* [9] measured the H^+-N_2 charge transfer differential cross section with high angular resolution for 0.5, 1.5, and 5.0 keV protons. No prior measurements of the direct scattering cross section have been made.

In this work, we provide calculations of the direct scattering and charge transfer cross sections for protons colliding with molecular nitrogen, as well as new experimental direct scattering measurements.

II. THEORETICAL SURVEY

A. Electron-nuclear dynamics

Our approach for studying the time dependence of a scattering process between a projectile and a molecular target is based on the application of the time-dependent variational principle (TDVP) [10], where the wave function is described in a coherent state representation. As the details of the electron nuclear dynamics (END) method have been reported elsewhere [11–13], only a brief summary of the basic features of the theory is given here.

The TDVP requires that the quantum mechanical action

$$A=\int \frac{\langle\psi|i\frac{\partial}{\partial t}-H|\psi\rangle}{\langle\psi|\psi\rangle}dt \tag{1}$$

should be stationary.

Application of the variational principle yields the time-dependent Schrödinger equation when variations of the wave function $|\psi\rangle$ over the entire state space are performed. Variation over a subspace yields the TDVP approximation of the Schrödinger equation for the time evolution over that subspace. We parametrize the wave function as a coherent state manifold, which leads to a system of Hamilton's equations of motion [11]. The variational wave function $|\psi\rangle$, is a molecular coherent state where the electronic and nuclear degrees of freedom are coupled. The END total wave function can be expressed as

$$|\psi\rangle=|z,\mathbf{R},\mathbf{P}\rangle|\mathbf{R},\mathbf{P}\rangle, \tag{2}$$

where $|z,\mathbf{R},\mathbf{P}\rangle$ and $|\mathbf{R},\mathbf{P}\rangle$ are the electronic and nuclear wave function, respectively. Here $\mathbf{R}$ and $\mathbf{P}$ are $3N$ dimensional arrays of the positions and momenta of all N nuclei and z is the time-dependent coefficient matrix that describes the electronic dynamics (*see below*).

The simplest level of the END approach employs a single spin unrestricted electronic determinant

$$|z,\mathbf{R},\mathbf{P}\rangle = \det\{\chi_i(\mathbf{x}_j,z,\mathbf{R},\mathbf{P})\}, \tag{3}$$

where $\mathbf{x}_j$ is the space-spin coordinate of electron j. The determinantal wave function is built from nonorthogonal dynamical spin orbitals

$$\chi_i = \phi_i + \sum_{j=N+1}^{K} \phi_j z_{ji}, \quad i=1,2,\ldots,N, \tag{4}$$

which, in turn, are expressed in terms of a basis of atomic spin orbitals $\{\phi_i\}$ of rank K, centered on the average positions $\mathbf{R}_k$ of the participating atomic nuclei and moving with a momentum $\mathbf{P}_k$. This representation takes into account the momentum of the electron explicitly through the electron translation factors (ETF) [14], which are required as the projectile energy reaches the ionization threshold. The particular form of parametrization of $|z,\mathbf{R},\mathbf{P}\rangle$ with complex, time dependent coefficients z_{ji} is due to Thouless [15], and is an example of a so called generalized coherent state [16].

The nuclear part of the wave function $|\mathbf{R},\mathbf{P}\rangle$ is represented by localized Gaussians or, in the narrow wave-packet limit, by classical trajectories $(\mathbf{R}_k,\mathbf{P}_k)$.

The resulting END equations are expressed in matrix form as [11]

$$\begin{pmatrix} i\mathbf{C} & \mathbf{0} & i\mathbf{C_R} & i\mathbf{C_P} \\ \mathbf{0} & -i\mathbf{C}^* & -i\mathbf{C}_\mathbf{R}^* & -i\mathbf{C_P}^* \\ i\mathbf{C_R}^\dagger & -i\mathbf{C}_\mathbf{R}^\mathbf{T} & \mathbf{C_{RR}} & -\mathbf{I}+\mathbf{C_{RP}} \\ i\mathbf{C_P}^\dagger & -i\mathbf{C}_\mathbf{P}^T & \mathbf{I}+\mathbf{C_{RP}} & \mathbf{C_{PP}} \end{pmatrix} \begin{pmatrix} \dot{\mathbf{z}} \\ \dot{\mathbf{z}}^* \\ \dot{\mathbf{R}} \\ \dot{\mathbf{P}} \end{pmatrix} = \begin{pmatrix} \partial E/\partial \mathbf{z}^* \\ \partial E/\partial \mathbf{z} \\ \partial E/\partial \mathbf{R} \\ \partial E/\partial \mathbf{P} \end{pmatrix}, \tag{5}$$

where

$$E = \sum_k \frac{P_k^2}{2M_k} + \frac{\langle z,R|H_{el}|R,z\rangle}{\langle z,R|R,z\rangle} \tag{6}$$

is the total energy of the system and H_{el} is the electronic Hamiltonian which contains the nuclear-nuclear repulsion terms. The nonadiabatic coupling matrix terms, the C's, between the electronic and nuclear dynamics are expressed in terms of the elements of the dynamical metric on the left. In particular,

$$C = \left.\frac{\partial^2 \ln S(z^*,R,P,z,R',P')}{\partial z^* \partial z}\right|_{R'=R,P=P'}, \tag{7}$$

$$C_R = \left.\frac{\partial^2 \ln S(z^*,R,P,z,R',P')}{\partial z^* \partial R'}\right|_{R'=R,P=P'}, \tag{8}$$

$$C_{RR} = -2\,\mathrm{Im}\left.\frac{\partial^2 \ln S(z^*,R,P,z,R',P')}{\partial R \partial R'}\right|_{R'=R,P=P'}, \tag{9}$$

with similar definitions for C_{RP}, C_P, and C_{PP}. Here, $\mathbf{C}$ describes the nonadiabatic coupling between the electronic degrees of freedom, $\mathbf{C_R}$ represents the nonadiabatic coupling of the electronic and nuclear degrees of freedom, $\mathbf{C_P}$ represents the nonadiabatic coupling of the electronic and nuclei momentum degrees of freedom and so on. These coupling terms are defined in terms of the overlap $S(z^*,R,P,z,R',P') = \langle z,R',P'|z,R,P\rangle$ of the determinantal states of two different nuclear configurations. When the effects of the electron translations factors are neglected, these sets of equation reduce to a simple form [17] with a purely classical equation of motion for the nuclear positions.

The END method has been implemented in the ENDyne program package [18] and its detailed theoretical foundations are given in Ref. [11]. Before presenting the details of the calculation for the $H^+ + N_2$ system we will describe how the differential cross section is obtained.

B. Direct differential cross section

Since the simplest level of END is based on the narrow width limit of the nuclear wave packets, it requires semiclassical corrections for the scattering process. We have implemented [19] the Schiff approximation [20] for small scattering angles which takes into account the quantum effects of the forward scattering. The advantage of using the Schiff approximation over some other semiclassical corrections (e.g., the Airy or uniform approximation) is that it includes all the terms of the Born series and treats the rainbow and glory angles in a single approach without requiring the separation into different scattering regions. The differential cross section is given by

$$\frac{d\sigma}{d\Omega} = \frac{k_f}{k_i}|f(\theta)|^2, \tag{10}$$

with

$$f(\theta) = ik_i \int_0^\infty [1-\exp(2i\delta(b))] J_0(qb) b\,db, \tag{11}$$

where $d\delta(b)/db = k_i\Theta(b)/2$. Here $\delta(b)$ is the phase shift, $\Theta(b)$ is the deflection function, such that $\theta = |\Theta|$ for the scattering angle, $q = |\mathbf{k}_f - \mathbf{k}_i|$, $J_0(x)$ is the Bessel function of order zero, and $\mathbf{k}_i$ and $\mathbf{k}_f$ are the initial and final wave vectors of the projectile, respectively.

In standard scattering theory, the phase shift $\delta(b)$ is determined through the interaction potential $V(r)$, where r is the projectile-target distance, thus requiring an analysis of the potential energy surface in a time-independent theory. In our case, we determine the phase shift at the end of the time-dependent collisions, by means of the deflection function for the projectile trajectory, $\Theta=\arccos(\mathbf{k}_f\cdot\mathbf{k}_i/k_fk_i)$, thus, incorporating dynamical effects, such as electron-nuclear coupling and charge transfer that occur during the collision. The deflection function therefore becomes the signature of the projectile-target collision and determines the shape of the differential cross section.

C. Charge transfer differential cross section

For the charge transfer process, the END model determines the final projectile charge state through the Mulliken population analysis [21–24].

In the linear combination of atomic orbitals method for electronic structure such as END, each electron in the system is described by a spin orbital

$$\chi_i(\mathbf{x})=\sum_\kappa c_{\kappa i}u_\kappa(\mathbf{x}) \tag{12}$$

as a sum over atomic basis orbitals $u_\kappa(\mathbf{x})$. The total electron charge density is then

$$\rho(\mathbf{x})=\sum_{\text{spin}}\sum_{\kappa,\lambda}\sum_{i=1}^{N} c_{\kappa i}c_{\lambda i}^{*}u_\kappa(\mathbf{x})u_\lambda^{*}(\mathbf{x})\,. \tag{13}$$

Integration of the charge density over all space yields the number of electrons $N=\Sigma_A n_A$, where the electron population on an atom A is defined as

$$n_A=\sum_{\kappa\in A}\sum_{\lambda}\sum_{i=1}^{N} c_{\kappa i}c_{\lambda i}^{*}(\delta_{\lambda\kappa}+S_{\lambda\kappa}) \tag{14}$$

with metric integrals $(\delta_{\lambda\kappa}+S_{\lambda\kappa})=(u_\lambda|u_\kappa)$, where $S_{\lambda\lambda}=0$. This is a good measure of the electronic atomic charge (probability) when the atoms are far apart, but is less meaningful when they strongly interact as this definition divides the overlap contributions equally between the two atoms involved. From the final number of electrons associated with atom A and the initial number of electrons, one determines the electron capture probability $P_e(b)$, as a function of the impact parameter, or the scattering angle through the deflection function $\Theta(b)$.

From the electron transfer probability, we calculate the electron transfer differential cross section as

$$\frac{d\sigma_{tr}}{d\Omega}=\frac{k_f}{k_i}P_e(\theta)|f(\theta)|^2 \tag{15}$$

for each orientation. Finally, we average over all the target orientations.

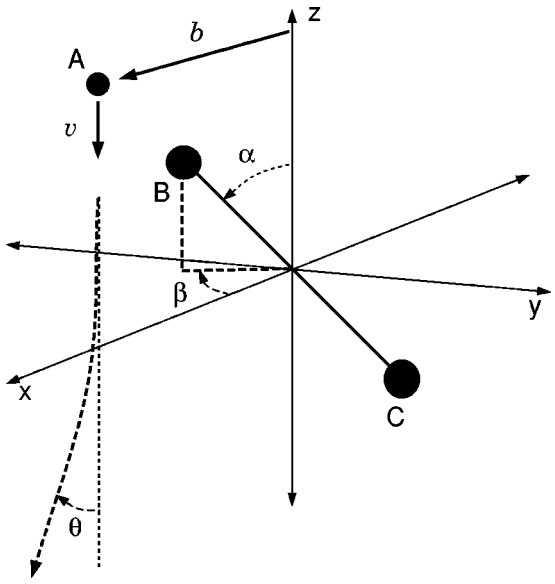

FIG. 1. Schematic representation of the initial conditions of the projectile-target system as required by the END approach.

D. Details of calculations

In order to perform the time-dependent analysis of the collision, the END approach requires the specification of initial conditions of the system under consideration. In Fig. 1, we show a schematic representation of the projectile-target arrangement. The initial projectile velocity is set parallel to the z axis and directed towards the stationary target with an impact parameter, b. In the case of atomic projectiles, as in this case, we need to consider the initial orientations of only the target. The target center of mass is initially placed at the origin of a Cartesian laboratory coordinate system and its orientation is specified by the angles α and β. For homonuclear diatomic molecules, we consider a minimum of three initial orientations of the target with respect to the direction of the incoming beam. These orientations yield a coarse set of grid points for rotational averaging. The three basic target orientations place the molecular bond along the x, y, and z axis. We will label these three orientations I $(\alpha=0,\beta=0)$, for the molecular bond aligned parallel to the incoming beam; II $(\alpha=90,\beta=0)$, for the molecular bond perpendicular to the beam, but with the impact parameter measured along the bond; and III $(\alpha=90,\beta=90)$ for the molecular bond perpendicular to the beam, as well as the impact parameter direction.

We perform the rotational average of a target property g as described in [25]. For the particular case of three orientations one obtains that

$$\bar{g}=\frac{1}{\pi}[(\pi-2)g_{\text{I}}+(g_{\text{II}}+g_{\text{III}})], \tag{16}$$

where g_i is the property of interest at orientation i.

The only limitation of the END approach, as in any other quantum chemistry treatment, is the restriction of a truncated Gaussian basis set used to describe the atomic orbitals $\{\varphi_i\}$. Although continuum wave functions and ionization can be

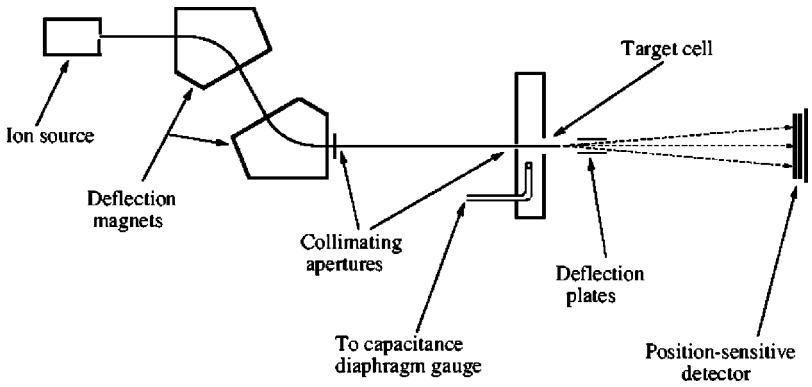

FIG. 2. Schematic of the scattering apparatus.

described with Gaussian functions, due to their expensive nature and their small contribution at these energies, we did not include the ionization channel in this work.

The molecular target is initially in its electronic ground state ($^1\Sigma_g^+$) and equilibrium geometry as computed in the given basis at the SCF level. The basis functions used for the atomic orbital expansion are derived from those optimized by Dunning [26,27]. For the hydrogen atomic structure, the basis set consists of $[5s2p/5s2p]$ with the addition of a diffuse s and p orbital for a better description of the long range interaction. For the N_2, the basis set consist of $[9s5p1d/3s2p1d]$ for each nitrogen atom. Thus, in the supermolecule description, these basis set give us a rank $K=35$ for each electron or $N\times K=490$ different time dependent z_{ij}'s Thouless coefficients to describe the electronic dynamics. We assign values to the impact parameter from 0.0 to 15.0 a.u. which we separate in three regions. For close collisions, from 0.0 to 6.0 a.u., we use steps of 0.1 a.u. For the intermediate region, from 6.0 to 10.0 a.u., we use steps of 0.5 a.u., and for $b>10.0$, we use steps of 1.0. This give us 74 fully dynamical trajectories for each target orientation and projectile energy.

The projectile starts 30 a.u. from the target, and the trajectory is evolved until the projectile is 30 a.u. past the target, or until there are no longer changes in the energy, velocity or charge of the projectile. Thus, after the dynamics is performed for each trajectory, one obtains the total wave function, the nuclei positions and momenta and therefore, one is able to calculate the deflection function Θ and electronic properties, e.g., charge transfer and energy loss.

III. EXPERIMENTAL APPROACH

The apparatuses employed for the present direct scattering measurements and for the earlier charge transfer measurements reported by Gao *et al.* [9] are very similar and may be represented schematically by Fig. 2. Both apparatuses and the techniques used have been described in detail previously [1,9,28] and are only discussed briefly here.[1] Ions are extracted from a low-pressure plasma-type ion source containing hydrogen, accelerated to the desired energy and focused by an electrostatic lens. Two confocal 60° sector magnets are used to select ions of the desired mass-to-charge ratio. Ions passing through a pair of laser drilled apertures form a beam with an angular divergence of approximately 0.02°. This collimated proton beam passes through a short target cell and impacts a position-sensitive detector (PSD) [29], located 26 cm beyond the target cell. The PSD serves to measure the flux of ions passing through the target cell and to measure the flux and positions of impact of scattered product species. An electric field established between a pair of deflection plates located between the target cell and the PSD is used to prevent ions from striking the PSD when required.

In order to measure the differential charge-transfer cross section, N_2 is admitted to the target cell and the angles of scatter of the neutral H atoms, formed by charge transfer of the primary H^+ ions, are determined from their positions of impact on the PSD. Unscattered primary H^+ ions are normally deflected from the PSD but are allowed to impact it periodically to assess the primary beam flux. These measurements, together with the target number density, obtained from the target gas pressure, and target length are sufficient to determine the absolute differential cross section.

A full account of the procedure for determining direct scattering differential cross sections has been given by Newman *et al.* [30]. Both the primary beam and scattered product species are allowed to impact the PSD. Essentially, the primary beam flux is the total flux of particles impacting the detector, while the flux of particles scattered at any angle θ is simply the flux of particles impacting an annular ring at that angle. In the present study the situation is more complex than this because, in addition to the primary and scattered H^+ ions, fast neutral H charge transfer products are also detected. It is therefore necessary to conduct an additional measurement to assess the number of H atoms produced and subtract this H atom signal from the total scattering signal to arrive at the scattered H^+ signal. As the charge transfer and direct scattering cross sections are comparable this procedure renders the H^+ direct scattering cross section more susceptible to systematic errors resulting in larger overall uncertainties than for the charge transfer measurements.

IV. RESULTS

A. Deflection function

As stated in Sec. II B, we require the deflection function to calculate the differential cross section. In Fig. 3, we show

[1]Note that the numerical values quoted are specific to the direct scattering apparatus.

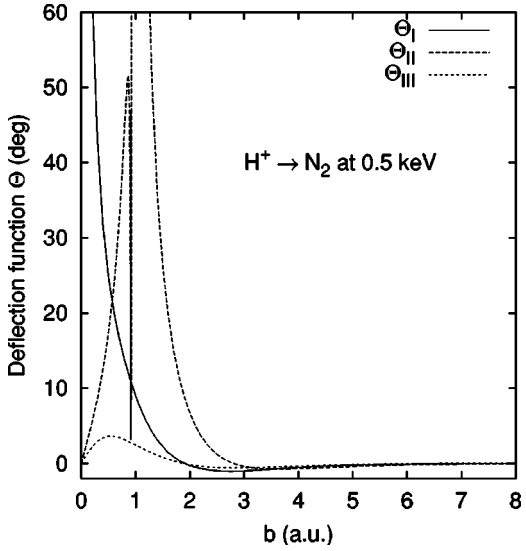

FIG. 3. Deflection function $\Theta(b)$ for H^+ colliding with N_2 at 0.5 keV for the three different target orientations.

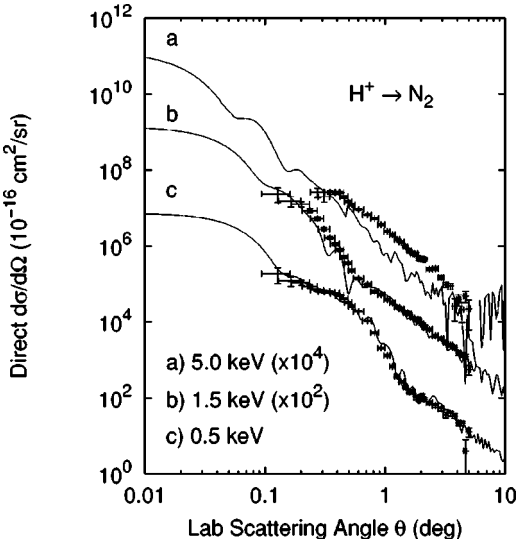

FIG. 4. Absolute direct differential cross section for protons colliding with molecular nitrogen for projectile energies of 0.5, 1.5, and 5.0 keV. The solid line represents our theoretical work and the circles with error bars are our experimental results. Note that, for clarity, the data are shown on different scales.

the deflection function for H^+ colliding with molecular nitrogen at 0.5 keV for the three different target orientations. For orientation I, the scattering angle shows a similar behavior to the atomic case, that is, at small impact parameters, the projectile experiences backward scattering as a consequence of the collision between the projectile and nitrogen B (head-on collisions) (see Fig. 1). Atom C only produces a small perturbation on the projectile trajectory after the projectile has interacted with atom B. For this orientation, the deflection function shows a glory angle ($\Theta_g=0$) for an impact parameter of $b_g=1.9$ a.u. and a rainbow angle ($d\Theta_r/db=0$) for $b_r=2.8$ a.u., with $\Theta_r=-1.05°$.

For orientation II, with the projectile impact parameter along the molecular bond, we note the following interesting effect. For $b<1.019$ a.u. which corresponds to impact parameters inside the molecular bond, the projectile is repelled as it gets closer to atom B. But as it does, the diatomic molecule rotates due to the interaction (rovibrational excitations). This produces a set of trajectories with the projectile colliding with atom B, then getting scattered at an angle that makes it collide with atom C and leave the system with a different scattering angle. This type of collision, produces a narrow dip in the deflection function for $b\sim0.9$ where Θ dips from 50° to less than 5°. For $b=1.019$ a.u. we have a head-on collision with atom B and for larger impact parameters we a have repulsive interaction until $b=2.8$ a.u. where a glory occurs. For $b=3.6$ a.u. we find a rainbow angle at $\Theta_r=-0.76°$.

For orientation III, with impact parameter perpendicular to the bond, we note from Fig. 3, that as the projectile moves, it is attracted at large impact parameters (long range interaction) and repelled at small impact parameters when the projectile has penetrated part of the target electronic cloud. In this orientation we have two rainbows: one at $b=0.55$ a.u. with $\Theta_r=3.62°$ and the second at $b=2.6$ a.u. with $\Theta_r=-0.59°$. A glory angle occurs at $b=1.9°$. Thus, the behavior of the deflection functions shown in Fig. 3 are a result of the dynamical interaction of the projectile and the molecular target, and do not represent a clamped target as in a stationary analysis.

We need to stress here that the deflection function discussed above is for all scattering processes, i.e., it includes all scattered projectiles independent of their charge state.

B. Direct differential cross section

We use the results for the dynamical deflection function in conjunction with the Schiff approximation [see Eq. (11)] to obtain the direct differential cross section. For this, from Eq. (11) we obtain the total differential cross section and the charge transfer differential cross section and subtract them. This produces the differential cross section for H^+, i.e., the direct differential cross section.

Figure 4 shows the calculated absolute direct differential cross section compared with our experimental results. We note that the use of the Schiff approximation gives the correct result for small angle scattering. We see more structure in the theoretical results than in their experimental counterpart. One reason for this is the coarse grid used for the target rotational average. For low energies, we note a large bump in the direct differential cross section for $\theta\sim0.6°$ which is a consequence of the rainbow scattering discussed in Sec. IV A.

C. Charge transfer differential cross section

The charge transfer cross section is determined using Eq. (15). In Fig. 5, we show the probability for electron capture by the proton projectile averaged over different target orientations for electron capture by the proton projectile, $\langle P_e(\theta)\rangle$, as a function of the scattering angle θ. Several instances of rainbow scattering can be clearly seen. For 0.5 keV the curve

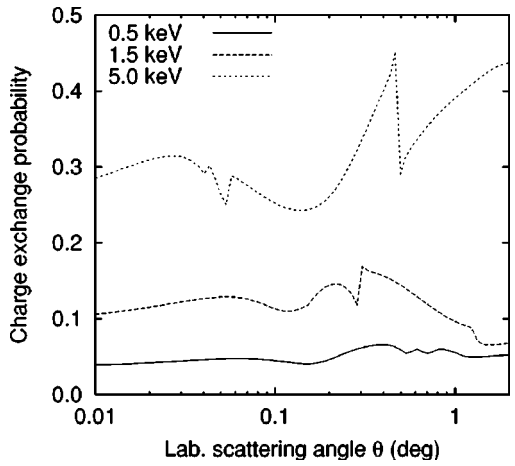

FIG. 5. Electron capture probability averaged over different target orientations for protons colliding with molecular nitrogen as a function of the scattering angle for the projectile energies indicated.

shows this effect at $\theta \sim 0.6°$. For 1.5 keV we see it at $\theta \sim 0.3°$ and $\theta \sim 1.05°$. For 5.0 keV, we see it at $\theta \sim 0.04°$ and $\theta \sim 0.5°$. Thus, the higher the energy, the smaller the rainbow angle, and the larger the electron capture probability.

The calculated charge transfer differential cross sections are shown in Fig. 6. These data are based on the Mulliken population (see Sec. II C) and therefore do not include interference effects for the probability amplitude. The experimental data from Gao *et al.* [9], for the three energies and from Quintana *et al.* [8] for 0.5 keV, are shown for comparison.

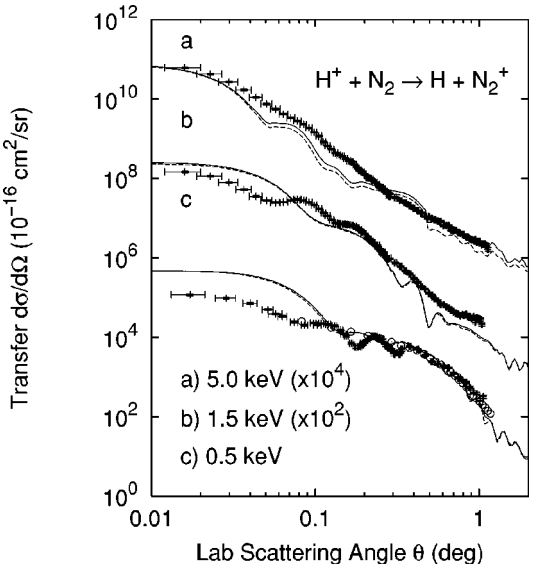

FIG. 6. Charge transfer differential cross section for protons colliding with molecular nitrogen for projectile energies indicated. The solid lines are the results for capture into all projectile states. The dashed lines, which closely follow the solid lines, are the results for electron capture into the H(1*s*) state only (see text). The experimental data are from ○, Gao *et al.* [9] and ×, Quintana *et al.* [8]. Note that, for clarity, the data are shown on different scales.

TABLE I. Integral direct and charge-transfer cross sections for $H^+ \rightarrow N_2$ as obtained by the END method and by experiment. The direct scattering measurements are the present results and the charge transfer measurements (*a*) are from Ref. [9]. Note also the results for the capture cross section into the 1*s* state of a hydrogen projectile.

		Angular	σ (10^{-16} cm^2)			
	Energy	range	END theory		Experiment	
$H^+ \rightarrow N_2$	(keV)	(deg)	H(1*s*)	Total		
Transfer	0.5	0.01−1.0°	4.17 (97%)	4.30	2.5[a]	
	1.5	0.01−1.0°	8.21 (95%)	8.67	8.1[a]	
	5.0	0.01−1.0°	7.00 (89%)	7.87	11.0[a]	
Direct	0.5	0.11−5.1°		24.12	21.8	±3.3
	1.5	0.11−5.1°		9.78	9.3	±1.4
	5.0	0.26−5.1°		0.62	1.28	±0.13

In Fig. 6 we also show the H(1*s*) capture contribution to the charge transfer differential cross section obtained through Eq. (15) by projecting the final projectile wave function into the 1*s* state of the projectile in the prescribed basis set. As previously found experimentally by Quintana *et al.* [8], the neutralized projectile is almost entirely in the ground state for the angular region considered here, i.e., small angles. However, at the highest energy studied, 5.0 keV, excited states start to become populated and contribute significantly to scattering at the larger angles.

At high energies, where the quantum interference effects are small, the agreement between theory and experiment is fairly good. For lower projectile energies quantum effects become important as shown by the 0.5 keV curve. This difference is the result of neglecting the interference effects in the scattering amplitude, as assumed in Eq. (15). A more proper description incorporates the probability amplitude for charge exchange. This is work in progress. In general, the theoretical curves follow the trend of the experimental data, giving us confidence in the dynamical description for the electron transfer process presented here.

D. Integral cross section

Integration of the electron transfer differential cross section over the scattering angles gives the integral electron transfer cross section. In Table I we present the results obtained with the END method and compare with the experimental data obtained by Gao *et al.* [9].

For the case of the direct differential cross section, we note that integrating over the experimental range gives a total cross section within 10% of the experimental value for low energies. The same trend is observed for the total electron capture cross section (exchange). However, the larger energy shows a greater discrepancy, the reason being the opening of the ionization channel and the lack of continuum states in our theoretical description.

V. CONCLUSIONS

Characterization of the dynamics in the collision of protons colliding with molecular nitrogen is carried out experi-

mentally and theoretically. For the theoretical analysis we use the electron-nuclear dynamics approach to approximate the time-dependent Schrödinger equation. We show that by using the Schiff approximation to include quantum interference effects in the description of the direct differential cross section, and by using the deflection function obtained through the dynamical END formalism, good agreement is obtained between theory and experiment. Good general agreement is also obtained for the electron transfer differential and total cross sections, where we find that at least 90% of charge transfer events result in the hydrogen atom leaving the system in the H($1s$) state.

ACKNOWLEDGMENTS

This work was supported partially by NSF (Grant No. CHE-973202 to N.Y.O. and E.D., No. CHE-9974385 to J.R.S., and No. ATM-0108734 to B.G.L.), by ONR (Grant No. N0014-97-1-0261 to N.Y.O. and E.D. and No. N0014-96-1-00707 to J.R.S.), and by an IBM SUR grant. This support is gratefully acknowledged.

[1] B. G. Lindsay, D. R. Sieglaff, D. A. Schafer, C. L. Hakes, K. A. Smith, and R. F. Stebbings, Phys. Rev. A **53**, 212 (1996).
[2] J. H. Moore, Jr., Phys. Rev. A **9**, 2043 (1974).
[3] J. H. Birely, Phys. Rev. A **10**, 550 (1974).
[4] V. M. Lavrov, M. R. Gochitashvili, V. A. Ankudinov, and B. I. Kikiana, Zh. Eksp. Teor. Fiz. **78**, 516 (1980).
[5] D. H. Loyd and H. R. Dawson, Phys. Rev. A **11**, 140 (1975).
[6] C. S. Lee and C. H. Lin, Phys. Rev. A **65**, 042712 (2002).
[7] E. W. McDaniel, J. B. A. Mitchell, and M. E. Rudd, *Atomic Collisions* (Wiley, New York, 1993).
[8] E. J. Quintana, V. R. Heckman, and E. Pollack, Phys. Rev. A **48**, 3670 (1993).
[9] R. S. Gao, L. K. Johnson, C. L. Hakes, K. A. Smith, and R. F. Stebbings, Phys. Rev. A **41**, 5929 (1990).
[10] Y. Öhrn, E. Deumens, A. Diz, R. Longo, J. Oreiro, and H. Taylor, *Time-Dependent Quantum Molecular Dynamics* (Plenum, New York, 1992).
[11] E. Deumens, A. Diz, R. Longo, and Y. Öhrn, Rev. Mod. Phys. **66**, 917 (1994).
[12] E. Deumens and Y. Öhrn, J. Phys. Chem. **92**, 3181 (1988).
[13] E. Deumens, A. Diz, H. Taylor, and Y. Öhrn, J. Chem. Phys. **96**, 6820 (1992).
[14] J. B. Delos, Rev. Mod. Phys. **53**, 287 (1981).
[15] D. J. Thouless, Nucl. Phys. **21**, 225 (1960).
[16] J. R. Klauder and B. S. Skagerstman, *Coherent States, Applications in Physics and Mathematical Physics* (World Scientific, Singapure, 1985).
[17] R. Cabrera-Trujillo, E. Deumens, Y. Öhrn, and J. R. Sabin, Nucl. Instrum. Methods Phys. Res. B **168**, 484 (2000).
[18] E. Deumens, T. Helgaker, A. Diz, H. Taylor, J. Oreiro, J. A. Morales, and R. Longo, ENDyne version 2.7 Software for Electron Nuclear Dynamics, Quantum Theory Project, University of Florida, 1998.
[19] R. Cabrera-Trujillo, J. R. Sabia, Y. Öhra, and E. Deumens, Phys. Rev. A **61**, 032719 (2000).
[20] L. I. Schiff, Phys. Rev. **103**, 443 (1956).
[21] R. S. Mulliken, J. Chem. Phys. **23**, 1833 (1955).
[22] R. S. Mulliken, J. Chem. Phys. **23**, 1841 (1955).
[23] R. S. Mulliken, J. Chem. Phys. **36**, 3428 (1962).
[24] R. Cabrera-Trujillo, Y. Öhrn, E. Deumens, and J. R. Sabin, Phys. Rev. A **62**, 052714 (2000).
[25] D. Jacquemin, J. A. Morales, E. Deumens, and Y. Öhrn, J. Chem. Phys. **107**, 6146 (1997).
[26] T. H. Dunning, J. Chem. Phys. **90**, 1007 (1989).
[27] D. E. Woon and T. H. Dunning, J. Chem. Phys. **100**, 2975 (1994).
[28] L. K. Johnson, R. S. Gao, C. L. Hakes, K. A. Smith, and R. F. Stebbings, Phys. Rev. A **40**, 4920 (1989).
[29] R. S. Gao, P. S. Gibner, J. H. Newman, K. A. Smith, and R. F. Stebbings, Rev. Sci. Instrum. **55**, 1756 (1984).
[30] J. H. Newman, K. A. Smith, R. F. Stebbings, and Y. S. Chen, J. Geophys. Res. [Space Phys.] **90**, 11 045 (1985).